Acta Crystallographica Section D
Biological Crystallography
ISSN 0907-4449

1.3 Å X-ray structure of an antibody Fv fragment used for induced membrane-protein crystallization

Lars-Oliver Essen,[a]* Axel Harrenga,[b] Christian Ostermeier[b] and Hartmut Michel[b]

[a]Department of Chemistry, Philipps University, Hans-Meerwein-Strasse, D-35032 Marburg, Germany, and [b]Max-Planck-Institute of Biophysics, Department of Membrane Biology, Heinrich-Hoffmann-Strasse 7, D-60528 Frankfurt/Main, Germany

Correspondence e-mail: essen@chemie.uni-marburg.de, hartmut.michel@mpibp-frankfurt.mpg.de

Received 30 September 2002
Accepted 24 January 2003

PDB Reference: unliganded 7E2 Fv fragment, 1mqk, r1mqksf.

The antibody Fv fragment 7E2 has previously been employed in the induced crystallization of the integral membrane protein cytochrome *c* oxidase from *Paracoccus denitrificans*. The 1.3 Å X-ray structure of the uncomplexed antibody fragment reveals conserved water networks on the surfaces of the framework regions. A novel consensus motif for water coordination, *XX*(S/T), is found along the edges of the β-sandwich, where a water molecule forms hydrogen bonds to the carbonyl O atom of a residue at position *N* and the OG hydroxyl groups of conserved serines or threonines at position $N + 2$. Multiple conformations were found in the hydrophobic core for residues IleL21, LeuL33 and the disulfide bridges. An internal water molecule that is compatible with only one of the three packing states of the V_L core suggests local 'breathing' of the variable domain. TrpH47, a conserved key residue of the V_H/V_L interface, is crucially involved in the formation of the antigen-binding site by adopting a novel conformation that specifically stabilizes the non-canonical CDR-L3 loop. Finally, a comparison with 7E2–cytochrome *c* oxidase complexes demonstrates that binding of this membrane-bound antigen proceeds without major conformational changes of the 7E2 antibody fragment.

1. Introduction

Antibodies have an interesting potential in structural biology by serving as tools for either protein purification (Kleymann, Ostermeier, Ludwig *et al.*, 1995) visualization (Kleymann, Ostermeier, Heitmann *et al.*, 1995) or crystallization (Hunte & Michel, 2002; Ostermeier, Iwata *et al.*, 1995). For the challenging three-dimensional crystallization of integral membrane proteins, cocrystallization with Fv or Fab fragments has proved to be an interesting alternative (Hunte & Michel, 2002) to other non-conventional methods such as crystallization in cubic lipidic phases (Landau & Rosenbusch, 1996) or nucleation on small-molecule crystals (Essen *et al.*, 1998; Schertler *et al.*, 1993). The high-affinity antibody 7E2 (mouse IgG_1,κ) was the first case where an Fv fragment was successfully used for crystallization of a membrane protein, cytochrome *c* oxidase (COX) from *Paracoccus denitrificans* (Ostermeier, Essen *et al.*, 1995; Ostermeier, Iwata *et al.*, 1995). Tetragonal cocrystals formed between this conformation-sensitive antibody fragment and a COX preparation comprising four subunits culminated in the first structure determination of an eubacterial COX (Harrenga & Michel, 1999; Iwata *et al.*, 1995). Subsequent cocrystallization with a two-subunit COX yielded orthorhombic crystals of significantly better quality (Ostermeier *et al.*, 1997). In both crystal forms the 7E2 Fv fragment acted as a molecular cornerstone in the macromolecular crystal lattice. In the tetragonal crystal

form of the COX–7E2 complex, all crystal contacts were formed by the Fv fragment (Ostermeier *et al.*, 1997; Ostermeier, Essen *et al.*, 1995). In the orthorhombic crystal form, the majority of crystal contacts were similarly contributed by the 7E2 Fv fragment.

The antigen-binding site of Fv fragments is generally built up of six hypervariable loops (CDR-L1, -L2, -L3, -H1, -H2 and -H3), which are grafted onto the conserved β-sandwich scaffolds of the variable domains. Structural comparison of antibody structures (reviewed in Padlan, 1994) showed that only a small set of canonical backbone conformations is required to describe five of the six CDR loops (Al-Lazikani *et al.*, 1997; Chothia *et al.*, 1992, 1989; Tomlinson *et al.*, 1995). This restricted structural repertoire facilitated the prediction and modelling of antigen-binding sites despite the large variation in CDR sequences (Chothia *et al.*, 1986; Martin *et al.*, 1989). A precise prediction of antigen-binding sites requires not only the accurate modelling of the CDR main-chain conformations, but also of their side chains and packing. Although antibody fragments belong to the protein families best studied by X-ray crystallography, only one of the 278 antibody structures deposited in the Protein Data Bank (as of September 2002) was determined at a resolution higher than 1.6 Å (PDB code 1a2y; 1.5 Å). As no antibody structure has been determined near the threshold of atomic resolution (1.2 Å), a concise view of the protein-bound solvent sphere and dynamic features of the protein region (Dauter *et al.*, 1997) is still missing. Likewise, the contribution of surface-bound waters to the conformation of the antigen-binding site or the V_H/V_L association is not completely understood.

Unlike other crystals of antibody fragments, crystals of the unliganded 7E2 fragment diffracted to close to atomic resolution (Ostermeier *et al.*, 1995). We determined the structure of the 7E2 Fv fragment by molecular replacement at 1.3 Å resolution. At this resolution, a large amount of structural flexibility was observed in the core region of the V_L domain. Database analyses identified water networks on the surface of the 7E2 Fv fragment which are conserved among Fv fragments and presumably affect the stability of variable domains. A detailed analysis of the 7E2–COX complex and its comparison with the uncomplexed 7E2 Fv fragment showed that CDR-L3, with its non-canonical conformation, plays an important role in antigen binding.

Table 1
Data-collection and refinement statistics.

(*a*) Data collection and processing. Values in parentheses are for the highest resolution shell.

Data set	I	II	I/II combined
Space group	$P2_12_12_1$	$P2_12_12_1$	$P2_12_12_1$
Unit-cell parameters (Å)			
a	51.12	51.44	51.44
b	55.61	56.05	56.05
c	99.09	99.85	99.85
Resolution (Å)	12.4–1.90	22.5–1.28	22.5–1.28
Wavelength (Å)	1.5418	1.0000	—
Observed reflections	114596	116276	178789
Unique reflections	21612	61408	64251
R_{merge}† (%)	3.7 (11.7)	4.8 (21.6)	4.0 (21.8)
Completeness (%)	93.0 (75.0)	81.4 (63.4)	85.1 (63.4)
Redundancy	5.3 (4.6)	2.1 (1.9)	2.8 (1.9)
$\langle I/\sigma(I)\rangle$‡	62.5 (23.7)	25.9 (5.2)	28.6 (5.2)
Wilson *B* factor (Å^2)	13.2	12.8	13.1

(*b*) Refinement.

Stage	1	2	3
Method	*X-PLOR*, isotropic	*SHELX*, isotropic	*SHELX*, anisotropic
Resolution	8.0–1.30	8.0–1.28	8.0–1.28
R factor† (%)	17.5	17.3	13.6
R_{free}‡ (%)	21.5	21.1	19.6
No. of reflections	60125	62275	64005
Observables/parameter	6.7	7.0	3.23
Weighted r.m.s.d. from ideality§			
Bond lengths (Å)	0.017	0.022	0.021
Bond angles (°)	1.38	2.49	2.28
Torsion angles (°)	28.7	28.6	28.1
Total No. of atoms	2148	2138	2130
Total No. of waters¶	336	326	318
Multiple conformers	27	27	23
Mean *B* value†† (Å^2)	19.8 (31.2)	23.5 (48.2)	22.8 (46.8)

† $R_{merge} = [\sum\sum|I_j(h) - \langle I(h)\rangle|/[\sum\sum I_j(h)] \times 100$. ‡ As calculated with the program *TRUNCATE* (Eigenbrot *et al.*, 1993). † $R = \sum||F_o| - k|F_c||/\sum|F_o|$, where k is a scaling factor. ‡ Free *R* factor calculated with 4% of data not included during refinement. § With respect to Engh & Huber parameters (Engh & Huber, 1991). ¶ Only non-H atoms. †† Values in parentheses are for waters.

2. Materials and methods

2.1. Crystallization

The expression, purification and crystallization of the 7E2 Fv fragment was performed as described in Ostermeier *et al.* (1995). The recombinant antibody fragment harbours a Cys→Ser mutation at position H50 that does not affect antigen binding but is required for high-level expression (Ostermeier, Iwata *et al.*, 1995). Crystals were obtained by microdialysis against low-salt conditions (12 mg ml^{-1} protein, 100 m*M* sodium phosphate pH 6.0, 277 K). Macroseeding was employed in order to obtain high-quality crystals reaching maximal sizes of 0.3 × 0.5 × 1.5 mm. The crystallization was reversible; warming to room temperature redissolved the Fv crystals. The Fv fragment crystallizes in space group $P2_12_12_1$, with unit-cell parameters a = 51.51, b = 56.15, c = 99.86 Å. The asymmetric unit contains one Fv fragment (MW = 27 542 Da) and has a solvent content of 53%(*v*/*v*) (Matthews, 1968).

2.2. Data collection and processing

Two data sets were collected at 277 K using a single crystal for each. Data set I was measured to 1.9 Å resolution on an 18 cm diameter imaging plate (MAR Research) using a Rigaku RU-200 rotating-anode generator (Cu $K\alpha$, 40 kV, 100 mA). Data set II was collected on the MPG-ASF beamline BW6 at the DORIS storage ring, DESY, Hamburg (λ = 1.0000 Å) on a 30 cm diameter imaging plate (MAR Research). Data were processed and integrated using *MOSFLM* (Collaborative Computational Project, Number 4, 1994). Scaling and data merging used the *CCP*4 suite programs *ROTAVATA* and *AGROVATA* (Collaborative

Computational Project, Number 4, 1994). The lack of completeness in the low-resolution shells of data set II required the merging of both data sets. The intrinsic temperature factors of the data sets were estimated by Wilson plots to be 12.7 and 13.2 Å^2, respectively. On the basis of the common Wilson statistics, the intensity data of data set I ($I > 2\sigma$; data in the resolution range 25–2.5 Å) and II ($I > 1\sigma$; 12.5–1.28 Å) were scaled together using *ROTAVATA*/*AGROVATA*. The final data statistics are shown in Table 1.

2.3. Structure solution

Sequence comparison of the 7E2 variable domains with those from 30 crystallographically characterized antibody fragments selected the V_L domain of the antibody 4D5 (PDB code 1fvc; Eigenbrot *et al.*, 1993) and the V_H domain of the antibody 17/9 (PDB code 1hil; Schulze-Gahmen *et al.*, 1993) as a search model. Besides sequence identities of 66% for V_L and 81% for V_H, the CDR loops L1, L2, H1 and H2 of these domains had the same lengths and similar sequences as in the 7E2 antibody. The model was used with data set I for real-space Patterson rotation searches in *X-PLOR* (Patterson vectors, 15–4.0 Å; structure factors, 15–3.5 Å). Patterson correlation refinement (Brünger, 1990) gave a clear peak for the 7E2 Fv fragment that corresponded to a rotation of the mass-centred search model by the Eulerian angles ψ, φ, κ = (149.6, 16.8, 102.2°). Translation searches on a 1.0 Å grid localized the Fv fragment at (0.34, 0.03, 0.09) with a correlation coefficient of 22σ (next peak 14σ; mean 7σ). At this stage, the *R* factor was 44.7% (data in the resolution range 8–2.5 Å) and decreased to 41.0% after rigid-body refinement.

2.4. High-resolution refinement

After sequence correction, positional and simulated-annealing refinement reduced the *R* factor to 28.4% (8.0–1.9 Å). The $2|F_o| - |F_c|$ electron-density map showed that CDRs L1, L2, H1 and H2 adopt the canonical conformations of their parental antibody structures. CDR-L3 and CDR-H3 were completely rebuilt in simulated-annealing omit maps. 135 water molecules were added stepwise until the *R* factor converged at 18.4%. This model of the 7E2(C50S) Fv fragment was used in structure determination of the 7E2–COX complexes (Iwata *et al.*, 1995; Ostermeier *et al.*, 1997). Refinement was continued with the combined high-resolution data set I/II. The solvent region was automatically updated using *ARP* (Lamzin & Wilson, 1993). *X-PLOR* refinement performed without electrostatic terms converged at an *R* factor and R_{free} of 17.5 and 21.5%, respectively, for data in the resolution range 8.0–1.3 Å and 336 water molecules (stage 1); the refinement was then continued by alternating *SHELX*93 and *ARP* cycles. The isotropic refinement converged with 326 water molecules at an *R* factor and R_{free} of 17.3 and 21.1%, respectively (stage 2). A slight improvement of the model by anisotropic refinement in *SHELX*93 was indicated by an initial fall in R_{free} to 20.1%. All waters with the exception of water W2 were refined with an occupancy of one; no waters with principal mean-square atomic displacements larger than 1.2 Å were kept. Anisotropic refinement converged at an *R* factor and R_{free} of 13.6 and 19.5%, respectively. In order to obtain estimated standard deviations for atomic positional and thermal parameters, the structure was finally subjected to full-matrix refinement with all data. 14 contiguous residue blocks were defined with an overlap of several residues. Estimated standard deviations are to some extent biased from the stereochemical library used, because restraints were not turned off to keep the refinement stable. Full-matrix refinement converged after four cycles at an *R* factor of 13.6% with 318 water molecules (stage 3).

2.5. Structural analysis

The numbering scheme for the V_L and V_H domains follows the convention of Kabat *et al.* (1991). Rigid-body superpositions of variable domains used *GA-FIT* with the recommended parameter set (May & Johnson, 1994). Connolly surfaces were calculated by *INSIGHT* II with a 1.7 Å probe to be consistent with previous surface analyses of antigen–antibody complexes (Davies & Cohen, 1996; Padlan, 1994). Structural comparison between the uncomplexed 7E2 Fv fragment and its complex with COX were only performed with the orthorhombic crystal form of the 7E2–COX complex (PDB code 1ar1) because this crystal form is structurally better defined than the tetragonal 7E2–COX crystals (Ostermeier *et al.*, 1997).

Analysis of solvent conservation was performed against a set of high-resolution antibody structures. 24 structures of Fv or Fab fragments which were solved at 2.1 Å resolution or better were selected from the PDB (PDB codes 1a2y, 1a3r, 1a4j, 1aj7, 1bfv, 1clo, 1dvf, 1fgv, 1flr, 1fvc, 1hil, 1hyx, 1igm, 1kel, 1mfb, 1mlb, 1nbv, 1osp, 1vfa, 1yec, 2fbj, 6fab, 7fab and 8fab). Owing to different V_H/V_L pairings, the following procedure was separately performed by an *X-PLOR* script for the V_H- and V_L-domain associated waters. (i) The variable-domain structures were superimposed with their solvent shells on the corresponding variable domain of the 7E2 Fv fragment. (ii) Water molecules were identified that resided within a 5 Å cushion around the variable 7E2 domain. Using this procedure, 1808 waters from the antibody set were stored as V_H-associated and 1401 as V_L-associated water molecules. (iii) Each water of the 7E2 Fv fragment was assigned to the V_H or V_L domain. The crystal symmetry-related mates were generated and the number of stored water molecules from the database that were within a radius of 1.2 Å around each water of the uncomplexed 7E2 Fv fragment was counted. The number of occurrences in the database was written to the *B*-factor column and the 7E2 waters were examined in *O* (Jones *et al.*, 1991) according to their colour-coded degree of conservation.

3. Results and discussion

3.1. Quality of the structure

The crystal structure of the uncomplexed 7E2 Fv fragment was refined at 1.28 Å resolution to an *R* factor and R_{free} of 13.6

and 19.5%, respectively, using the *SHELX*93 suite. The final model comprises 231 of 247 residues, L1–L108 and H1–H118 (numbering scheme according to Kabat *et al.*, 1991). Most of the final model is well defined by electron density, especially the CDR regions, which show electron density which has sufficient atomicity to unambiguously define the backbone and side-chain conformations (Fig. 1). However, no density was found for the polar *c-myc* tag (GluL109–MetL119) that was fused to the C-terminus of the V_L domain in order to allow immunodetection (Kleymann, Ostermeier, Heitmann *et al.*, 1995). Likewise, the Strep tag of the V_H domain (SerH113–GlyH122), which was used for the affinity purification of the Fv fragment and its cocomplex with cytochrome *c* oxidase on streptavidin-loaded Sepharose (Kleymann, Ostermeier, Ludwig *et al.*, 1995), was only defined to ProH118. Despite the high resolution, 11 residues which are exposed to the solvent are poorly defined, showing no or only partial electron density for their polar side chains; GlnL40 even shows a break in the main-chain electron density. Multiple conformers were modelled for 10% of the structurally defined residues (23/231). 17 of these residues are solvent-exposed and mostly polar; six residues with alternative conformers are found in hydrophobic regions that are completely buried from solvent access. IleL21 was modelled in three alternative conformations; the other residues, such as the N-terminus of the V_H domain, GluH1, were built with two conformers. The accuracy of this antibody structure is reflected by mean coordinate errors of the 7E2 Fv fragment of 0.10 or 0.07 Å as estimated by Luzzati and *SIGMAA* plots.

The overall stereochemical quality of the structure was analyzed by *PROCHECK* (Laskowski *et al.*, 1993) and *X-PLOR* (Brünger, 1993) (for statistics see Table 1). 90.2% (175) of all residues occupy the most favoured regions of the Ramachandran plot; only AlaL51 in CDR-L2 and TyrH98 in CDR-H3 reside in disfavoured regions.

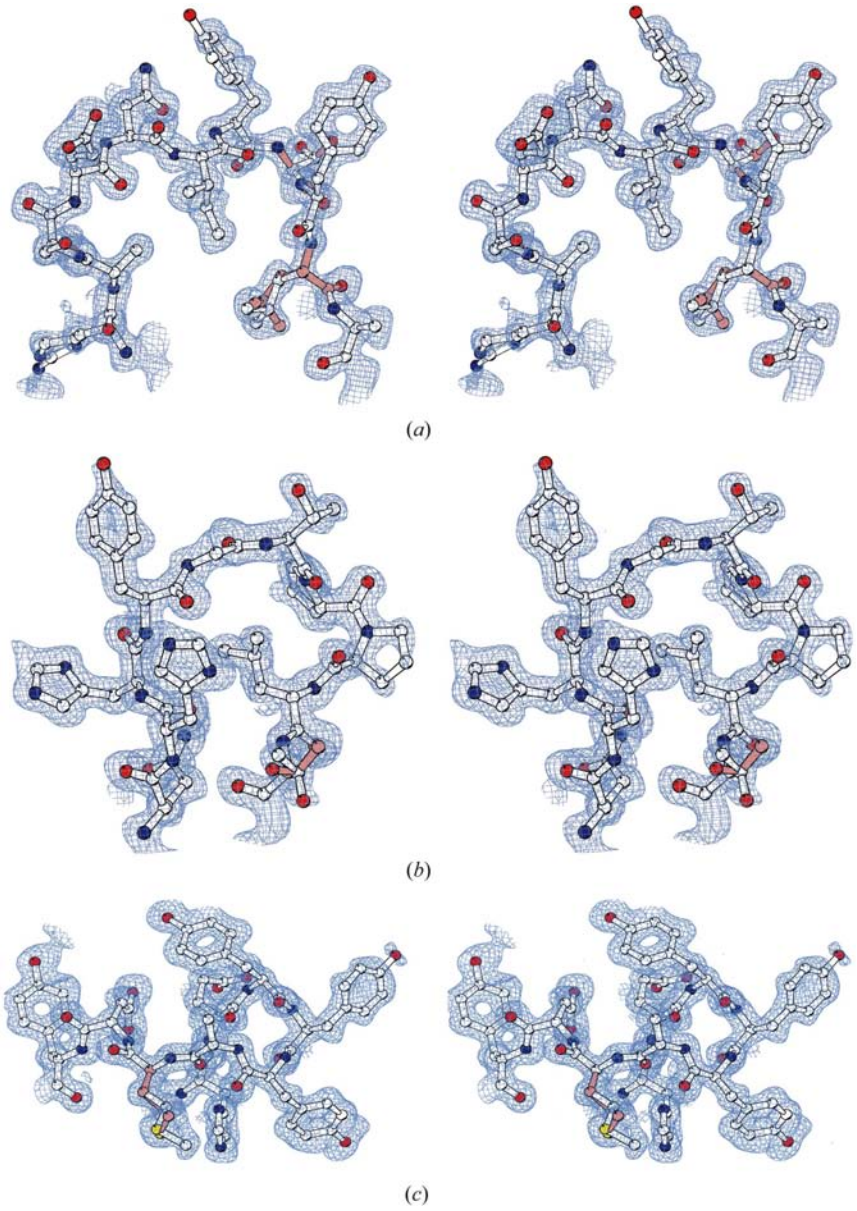

Figure 1
Stereoview of the $3|F_o| - 2|F_c|$ electron-density map of (*a*) CDR-L1, (*b*) CDR-L3 and (*c*) CDR-H3 after *SHELX*93 refinement (contouring level 0.4 e$^-$ Å^{-3}). Alternative side-chain conformers are shown in pale red. This figure and Figs. 2, 4 and 5 were generated by *BOBSCRIPT*, a modified version of *MOLSCRIPT* (Kraulis, 1991).

3.2. E2 CDR loop conformations

Four of the six CDR loops (L1, L2, H1 and H2) adopt the main-chain conformations of one of the major canonical classes that are usually observed in antibody structures (Al-Lazikani *et al.*, 1997; Chothia *et al.*, 1989, 1992): CDR-L1 (residues ArgL24–AlaL33) belongs to canonical class 2A that is anchored to the hydrophobic core of the V_L domain *via* the side chain of IleL29. IleL29 is in van der Waals contact with LeuL33 in the hydrophobic core, which adopts two different conformations along the χ_2 torsion angle and contacts the flexible disulfide bridge of the V_L domain (see below). The alternative conformers of the side chain of SerL31 are involved in two different hydrogen-bonding networks, one to W207 (2.5 Å) and W215 (2.4 Å) and the other to W104 (2.5 Å). The backbones of CDR-H1 (SerH31–SerH35) and CDR-L2 (AsnL50–GluL56) have canonical class 1 conformations. The two alternative conformers of GluL56 on CDR-L2 make hydrogen bonds either to TyrH102 OH (3.4 Å) of CDR-H3 or to water molecule W284 (2.6 Å). CDR-H2 (SerH50–GlyH65) has a class 3A conformation; the alternative side-chain conformations of AsnH52A of this CDR provide inter-CDR hydrogen bonds to either ThrH33 OG1 (3.4 Å) or to protein-bound waters W92 and W259.

CDR-H3 connects β-strands *F* and *G* and shows the highest conformational variability in the antibody structures. The non-canonical CDR-H3 of the free 7E2 Fv fragment (HisH95–TyrH102) and its complex with COX corresponds to a kinked long β-hairpin loop which packs along the V_H/V_L interface. Its stem region (CysH92–HisH95 and AlaH100–TyrH102) adopts an extended conformation that is common to other antibodies with at least 11 amino acids between H92 and H102 (Morea *et al.*, 1998; Shirai *et al.*, 1996). This stem carries a loop segment whose backbone conformation between GluH96 and AlaH100 closely agrees with the 3:3 loop classified by Sibanda *et al.* (1989). A hallmark of 3:3 loops is the presence of a residue at the +2 position which adopts a backbone conformation in the disallowed region of the Ramachandran plot. In the case of CDR-L2, which also belongs to the 3:3 loops, this residue is the highly conserved AlaL51 ($\varphi = 69$, $\psi = -34^\circ$) which donates a hydrogen bond to the conserved water molecule W1. Likewise, TyrH98 at the tip of the long segment of CDR-H3 occupies an energetically unfavourable backbone conformation ($\varphi = 67$, $\psi = -103^\circ$) which is apparently stabilized by three hydrogen bonds to CDR-L3: TyrH97 O–HisL91 ND1 (2.93 Å), TyrH99 N–HisL91 O (2.93 Å) and TyrH99 O–GlnL89 NE2 (2.99 Å).

With a length of seven instead of the usual six amino acids, CDR-L3 (GlnL89–ThrL97) adopts a conformation different from the five canonical structures currently known for CDR-L3. For CDR-L3 loops with seven residues, the only example is that of the murine antibody fragment AN02 (Brünger *et al.*, 1991), which alone represents the fifth canonical class of CDR-L3 loops (Tomlinson *et al.*, 1995). The antibodies 7E2 and AN02 have two of three key residues in common, ProL95A and ThrL97, but they differ at L90 (His in 7E2 and Gln in AN02; Tomlinson *et al.*, 1995). The CDR-L3 conformations are consequently different in these two antibodies, *e.g.* the $C^\alpha-C^\alpha$ distances for proline residues at L95 and L95A are 6.2 and 3.0 Å, respectively (Fig. 2*a*). In the 7E2 Fv fragment, this loop is involved in extensive CDR–CDR interactions with CDR-H3 and CDR-L2, mostly by tight side-chain packing of a surface-exposed tyrosine cluster comprising TyrL32, TyrL92 and TyrH98. This implies the existence of at least two canonical conformations for CDR-L3 loops longer than six residues. The CDR L3 and H3 loops of the 7E2 Fv fragment play an important role in stabilizing the V_H/V_L heterodimer: 48% of the 134 atoms engaged in the formation of the V_H/V_L interface are derived from CDR-L3 (23 atoms) and CDR-H3 (41 atoms); only CDR-H2 makes a minor contribution to the V_H/V_L interface by packing the aromatic side chain of TyrH59 against ProL95 of CDR-L3.

The peculiar conformation of CDR-L3 is strongly affected by TrpH47, a conserved key residue of the V_H/V_L interface (Fig. 2*b*). In the 7E2 Fv fragment, the indole moiety of TrpH47 points into the centre of the V_H/V_L interface ($\chi_1 = -146$, $\chi_2 = -83^\circ$), while in all other antibody structures, including the Fab fragment of AN02, the indole points outward ($\chi_1 \simeq 180$, $\chi_2 \simeq 80^\circ$). The unexpected conformer of TrpH47 causes multiple hydrophobic packing interactions with CDR-L3, in particular the pyrollidine groups of ProL95 and ProL95A. The aromatic side chain of TrpH47 participates in an internal hydrogen-bonding network among the CDR-H1, CDR-H2 and CDR-H3 loops of the V_H domain that consists of the interactions between TrpH47 NE1 and SerH50 OG (2.8 Å), SerH50 OG and SerH35 OG (2.6 Å) and between SerH35 OG and HisH95 NE2 (2.7 Å). The preservation of the CDR-L3 and TrpH47 conformations in the crystallographically determined complexes with COX (Harrenga & Michel, 1999; Ostermeier *et al.*, 1997) indicate that this structural feature is essential for antigen recognition. Variants of the 7E2 Fv

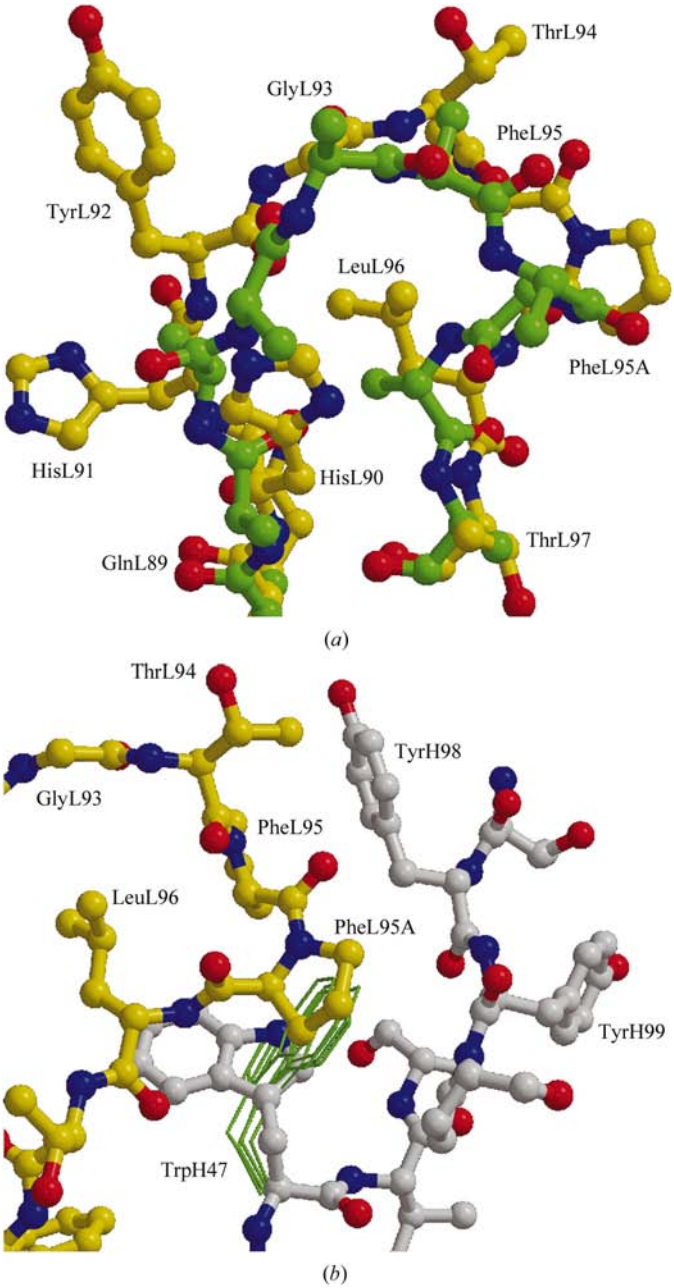

Figure 2
(*a*) Structural comparison between the CDR-L3 loops of the antibodies 7E2 and AN02. (*b*) Packing interactions of TrpH47 and CDR-L3. The numbering scheme for the V_L and V_H domains follows the convention of Kabat *et al.* (1991). Variable domains were superpositioned with *GA-FIT* (May & Johnson, 1994).

fragment in which the sequence was altered in CDR-L3 and CDR-H3 to introduce artificial metal-binding sites show that TrpH47 flips back to a standard conformation with concomitant structural changes for CDR-L3 and CDR-H3 (LOE, unpublished data). Together with the hypervariable CDR-H3 loop, CDR-L3 forms the central region of most antigen-binding sites. Large structural variability of long CDR-L3s should significantly enhance the diversity of antigen-binding sites and might be modulated more by CDR–CDR interactions with CDR-H3 than is observed for the six-residue CDR-L3 loops. With an occurrence of 18% in the human V_κ repertoire (Tomlinson *et al.*, 1995), CDR-L3s with seven residues are well represented in humans, but relatively rare in mice, with an occurrence of about 2.6% (Kabat *et al.*, 1991). Our observations on CDR-L3 conformations suggest that a larger set of canonical structures for long CDR-L3 loops might be required to predict the antigen-binding sites of a significant proportion of human antibodies.

3.3. Conserved solvation spheres of Fv fragments

Owing to the high resolution, the water model of the 7E2 Fv fragment is highly complete compared with other antibody structures. Therefore, it might be wondered whether there are any conserved water networks on the surface of the antigen-binding fragment and how these networks might correlate with conserved structural features of the protein. Two of the 318 water molecules which were included in the final model are completely buried from solvent access in the interior of the Fv fragment (W1, W2) and are discussed below. The other 316 waters cover 54% of the surface of the Fv fragment (4615/8568 Å^2). We performed a database survey in order to discriminate which of these solvent-exposed water molecules are routinely observed in well refined antibody structures or belong to waters unique to the 7E2 Fv fragment and its orthorhombic crystal form. As shown in Fig. 3(*a*), the vast majority of solvent-exposed waters lack related water molecules in other antibody structures (114/316) or are found in only one to three other structures (133/316). The large number of non-conserved water molecules reflects the local differences on the protein surfaces that are caused by crystal packing, crystallization media and structural deviations arising from sequence differences. However, 39 waters are found to be structurally conserved by being located at equivalent positions in seven or more high-resolution antibody structures. Furthermore, we observe a correlation between the degree of conservation and the thermal mobility of the water molecules in the 7E2 structure (Fig. 3*b*). Almost all the conserved waters are well ordered and have average *B* factors of 30 Å^2. This correlation between conservation and structural order indicates that the surface binding of these waters depends on conserved surface features of the variable domains.

12 water molecules are not only observed with high abundance in other antibody structures, but are also conserved between the V_H and V_L domains of the 7E2 Fv fragment. Three pairs (W19/W26, W21/W24 and W27/W94) are bound between the β-strands *A* and *B* and two pairs (W12/W37, W18/W65) are bound between the β-strands *E* and *F* of the variable domains (Table 2). The common binding motif for these water molecules consists of two hydrogen bonds towards the carbonyl O atom of residue *N* and the OG/OG1 atom of residue *N* + 2, which is a highly conserved serine or threonine residue of the framework region (Figs. 4*a* and 4*b*). Superposition of the peptide groups of residue *N* shows a clustering of the bound water molecules with an r.m.s.d. of 0.72 Å ($n = 9$).

There are three water networks which are conserved between the different antibody structures (Figs. 4*c* and 4*d*). Water network I (W9, W13, W30 and W60) resides between the β-strands *X* and *E* of the V_H domain and seals the β-sandwich of this variable domain along the edge of the

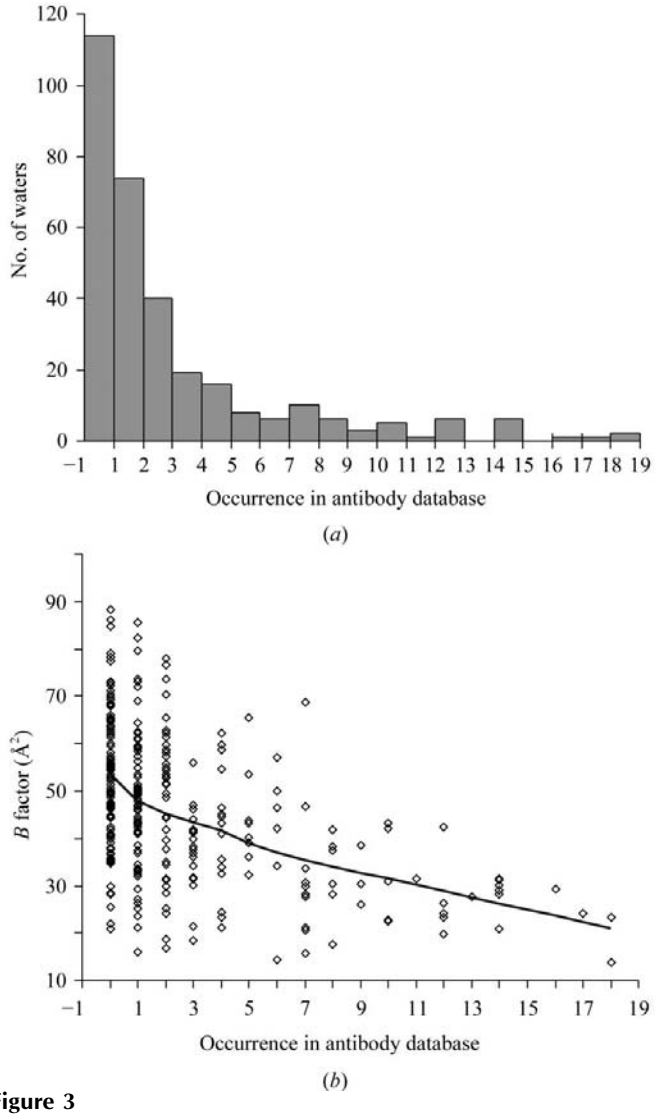

Figure 3
Conservation of water molecules on the surfaces of the variable domains. (*a*) Plot of the degree of conservation of water molecules in the 7E2 Fv structure as counted by the number of waters in the high-resolution database which are closer than 1.2 Å. (*b*) Plot of the degree of conservation of each water in the 7E2 structure against its *B* factor. (*c*) View along the C—O bond of the peptide group of residue *N*; (*d*) view perpendicular to the peptide group of residue *N*. Water molecules are shown in cyan; amide N atoms of the neighbouring β-strand to which the carbonyl O atoms of residue *N* form hydrogen bonds are highlighted in blue.

Table 2
Conserved water molecules of the 7E2 Fv fragment.

Water	Occurrence	Hydrogen bonding to	Distance (Å)	Comment
W1	18	TrpL35 NE1	3.0	Buried water, important for CDR-L2
		AlaL51 O	2.8	conformation
		SerL65 O	3.1	
W2	6	GlnL6 NE2	2.7	Buried water, part of flexible V_L core,
		ThrL22 O	3.0	only compatible
		ThrL102 OG1	2.8	with conformer *C* of IleL21
W5	7	HisH95 O	2.8	Water link between CDR-H1 and the stalk
		ThrH33 O	3.0	of CDR-H3
W6	8	PheL46 N	3.0	V_H/V_L interface
		AspH101 O	2.8	
W9	12	ArgH71 N	3.0	Water network between β-strands
		W60	2.8	*X* and *E* of V_H domain
+ W13	10	ThrH57 OG1	3.0	
		TyrH59 OH	2.7	
		W30	2.8	
+ W30	7	IleH69 O	2.7	
		W60	2.8	
+ W60	6	GlyH54 O	2.7	
W12	14	ThrH69 O	3.0	Between β-strands *E* and *F* of the
		SerH71 OG1	2.8	V_H domain
W14	12	AspL82 OD1	2.8	Conserved salt bridge
		GlnL37 NE2	2.7	between AspL82 and ArgL61
W17	14	W23	3.2	Water network between β-strands
		GlyL101 O	2.8	*A* and *H* of V_L domain
+ W23	13	GlyL6 N	3.0	
		GlyL100 N	2.9	
+ W33	14	LeuL4 N	3.1	
		ThrL97 OG1	2.5	
		PheL98 O	3.0	
		W225	3.4	
+ W225	4	LeuL4 O	2.7	
W18	9	ArgL61 O	3.0	Between β-strands *E* and *F* of the
		SerL63 OG	2.8	V_L domain
W19	14	GluL3 O	3.2	Between β-strands *A* and *B* of the
		ThrL5 OG1	2.8	V_L domain
W20	18	LysL52 O	2.8	Between stalk of CDR-L2 and
		GlyL64 N	3.0	β-strand *E* of V_L domain
W21	11	ThrL5 O	3.0	Between β-strands *A* and
		ThrL7 OG1	2.8	*B* of the V_L domain
W24	16	GlnH5 O	2.9	Between β-strands *A* and
	16	SerH7 OG	3.0	*B* of the V_H domain
W26	12	AlaH23 O	3.0	Between β-strands *A* and
		SerH25 OG	3.0	*B* of the V_H domain
W27	9	LysH19 O	2.9	At the beginning of pairing between
		SerH21 OG	2.7	β-strands *A* and *B* of the V_H domain
W32	17	LeuH4 N	3.1	Between β-strands *A* and *H*
		LeuH4 N	3.1	of the V_H domain
W36	9	AspL1 OD1	2.8	Connection between CDR-L1 and
		SerL26 OG	2.6	N-terminus
		GluL27 OE2	3.0	
W37	12	SerL65 OG	3.1	Between β-strands *E* and *F*
		SerL72 OG	3.2	of the V_L domain
W43	14	GluH85 O	3.2	Bound to backbone of *FG* loop
		ThrH87 O	2.7	
W65	8	ArgH66 O	3.1	Between β-strands *E* and
		ThrH68 OG1	3.0	*F* of the V_H domain
W148	8	PheL98 O	2.8	Water network between
		W158	3.0	the stalk of CDR-L3 and
		W318	3.2	β-strand *D* of the V_H domain
+ W155	14	PheL98 N	3.0	
		W158	3.0	
		W276	2.8	
+ W158	4	ArgH44 NH2	3.0	
		LeuH45 O	2.7	
+ W276	10	TrpH47 N	3.0	
		LeuL96 O	2.9	
+ W318	12	LeuH45 N	2.9	
		GlyL99 O	2.8	
W256	8	GlyH15 N	2.6	Between β-strands *B* and
		SerH82B N	2.9	*F* of the V_H domain

ABEF and *CDXGH* β-sheets. Likewise, water network II (W17, W23, W33 and W225) fills the other edge of the β-sandwich between β-strands *A* and *H* of the V_L domain and links the backbone of LeuL4–GlnL6 to the β-bulge at GlyL100–GlyL101. In the V_H domain, only W32 is found at an analogous position to W33 of water network II; the other waters of network II are missing owing to slight structural differences between the variable domains, *e.g.* the side chains of GlnH5 and GlnH105 hydrogen bond to each other and thereby close the edge of the β-sandwich. The third water network links the C-terminal stalk of CDR-L3 to β-strand *D* of the V_H domain. Other conserved water molecules which might also play a role in the stabilization of CDR loop conformations are W5, which sits between CDR-H1 and CDR-H3, and W20, which links the stalk of CDR-L2 towards the *E* strand of the V_L domain. The water molecule W36 cross-links the N-terminus of the V_L domain with the side chains of SerL26 and GlnL27 of CDR-L1. Sequence variations at these positions of CDR-L1 might therefore cause a slightly different placement of the N-terminus next to the antigen-binding site.

3.4. Hydrophobic core mobility

The high resolution of the electron-density maps unambigously revealed structural heterogeneity in the hydrophobic cores of both variable domains. The disulfide bridges inside the V_H and V_L domains adopt two alternative conformations: a right-handed conformation, which is mostly found in variable immunoglobulin domains with a positive S—S torsion angle $\chi_S \simeq +90^\circ$ (Richardson, 1981), and a left-handed conformation with a negative torsion angle $\chi_S \simeq -90^\circ$ (Fig. 5). According to the refined occupancies of these conformers (V_L, 0.72/0.28; V_H, 0.58/0.42), the energetic difference between the left- and right-handed conformers must be smaller than 2 kJ mol^{-1}. The structural flexibility does not involve topologically equivalent residues. In the V_L domain (Fig. 5*b*), CysL23 on β-strand *B* adopts *gauche*$^-$ and *trans* conformers ($\chi_1 = -99.6$ or -178.8°), whereas in the

V_H domain (Fig. 5*a*) CysH92 on β-strand *G* is found in *gauche*$^+$ and *trans* conformations (χ_1 = 65.2 or 159.5°). This non-equivalence might be caused by small differences in the packing and dynamics around the disulfide bridges, although the environment is otherwise highly conserved (TrpL35/TrpH36, GlnL6/GluH6 and LeuL34/MetH34). The two conformers of CysL23 occupy a volume very similar to a valine residue. Previous protein-engineering studies aimed towards the removal of the disulfide bridges in the REI V_L domain (Frisch *et al.*, 1996) or the V_L domain of the antibody ABPC48 (Proba *et al.*, 1998) have shown that CysL23 can indeed be replaced by valine or alanine. Accordingly, mutations of CysL88 to residues larger than alanine failed to yield stably folded protein.

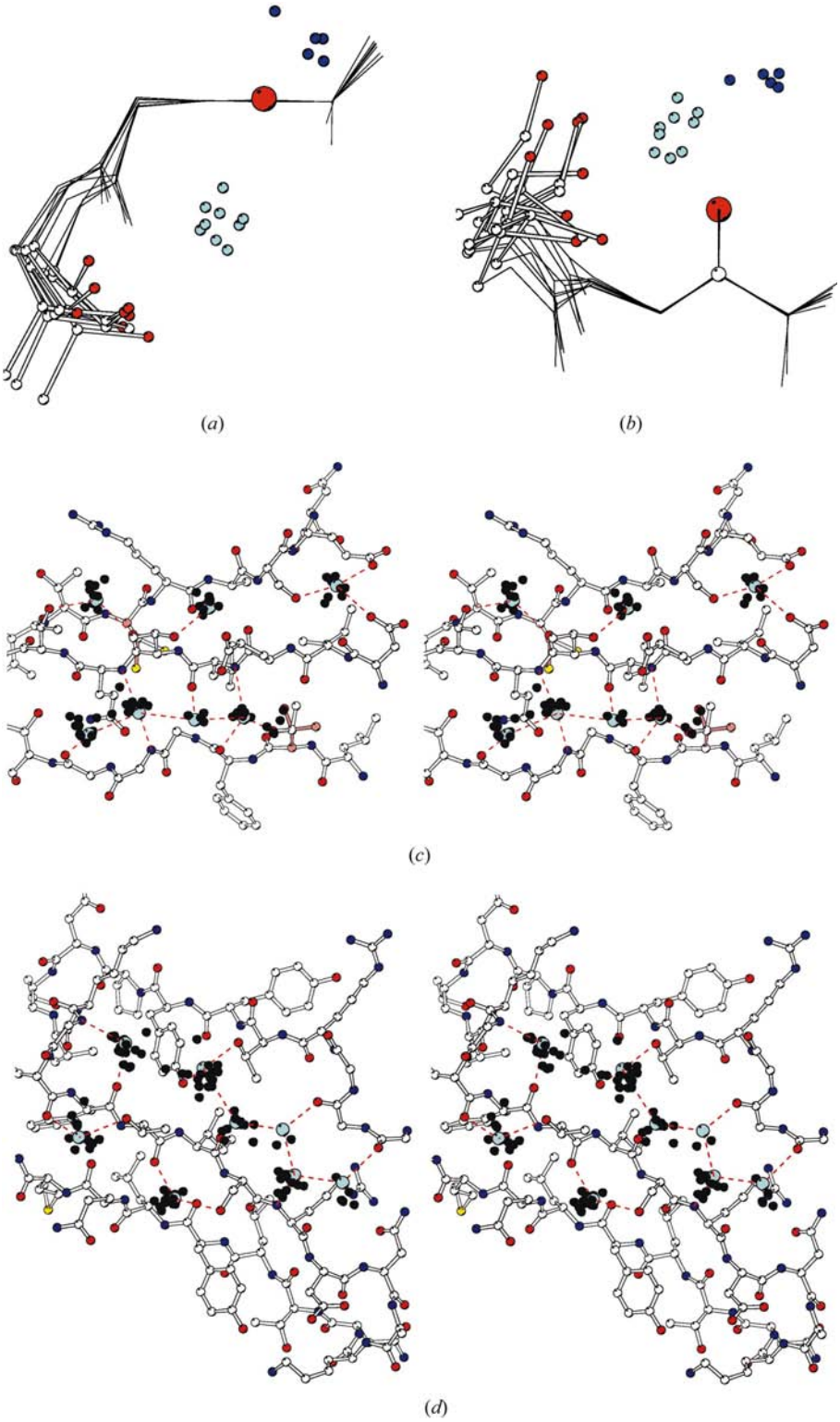

Figure 4
Highly conserved water networks on the surface of the framework reigons. (*a*) Conserved water network between β-strands *A*, *B* and *H* of the V_L domain. (*b*) Conserved waters between the β-strands *A*, *B* and *H* of the V_H domain. 7E2 waters are shown as cyan spheres, equivalent waters in the high-resolution database of antibody structures are highlighted as small black spheres (cutoff radius 2.5 Å) and conserved hydrogen bonds are shown as red dashed lines.

Unlike the V_H domain, the V_L domain reveals further 'breathing' mobility of the hydrophobic core surrounding the disulfide bridge CysL23–CysL88 (Fig. 5*b*). The isopropyl group of the core residue LeuL33 contacts the disulfide bridge and IleL29 of CDR-L1 and adopts two different conformers (χ_1/χ_2 = −170/89, −160/−78°). Three distinct rotamers (*A*, *B* and *C*) were crystallographically delineated for the core residue IleL21. This residue is not involved in van der Waals contacts with the disulfide bridge, but is a neighbour of water molecule W2, which is completely buried from the protein surface and resides halfway between IleL21 and CysL23. Water W2 is only partially occupied and forms hydrogen bonds with the side chains of GlnL6 (2.7 Å), ThrL103 (2.8 Å) and the carbonyl O atom of ThrL22 (3.0 Å). Owing to steric conflict with the side chain of IleL21 conformers *A* and *B*, the presence of the W2 water is only compatible with conformer *C*, with which it shares the crystallographic occupancy. So far, only water molecule W1, which makes hydrogen bonds to TrpL35 NE1 (3.0 Å) and the carbonyl O atoms of AlaL51 (2.8 Å) and SerL65 (3.1 Å), has been described as a structural feature that is strictly conserved among V_κ domains (Steipe *et al.*, 1992), while water molecule W2 was observed only in a few well resolved crystal structures, *e.g.* the anti-galactane antibody J539 (Suh *et al.*, 1986) or the V_L domain of McPC603 (Steipe *et al.*, 1992). Interestingly, single aspects of the alter-

native core states of the 7E2 structure have been recognized in previous crystal structures. Alternative conformers for the disulfide bridges of variable domains were firstly described in the V_L domain of REI (Epp *et al.*, 1974) and the V_H domain of a llama antibody (Spinelli *et al.*, 1996). The extent of structural heterogeneity that is observed in the variable domains of 7E2 suggests that the failure to identify crystallographically multiple core states in other antibody structures might simply be caused by a lack of high-resolution data and the low occupancy of alternative conformations. Earlier NMR studies of isolated V_L domains support this view by showing a considerable dynamic freedom in the cores of variable domains (Constantine *et al.*, 1993, 1994). However, the NMR data were not able to resolve structural details of the conformational heterogeneity. Structural flexibility is also observed in the V_H/V_L interface of the 7E2 Fv fragment, where ValH37 and MetH100A adopt two alternative conformers. This flexibility might be caused by packing imperfectness in the V_H/V_L interface which compensates for the tolerance towards amino-acid exchanges in the interface region.

3.5. The antigen-binding site

The overall flat nature of the antigen-binding site of the 7E2 Fv fragment mirrors the topological characteristics of its epitope on subunit II (SU II) of COX. This COX subunit is a globular ten-stranded β-barrel domain that belongs to class I copper proteins such as azurin and plastocyanin and is fused to an N-terminal membrane anchor comprising two transmembrane helices (Ser*B*25–*B*105; for the nomenclature of secondary-structure elements in COX, see Iwata *et al.*, 1995). The epitope on SU II is discontinous and comprises four regions (*B*26–*B*30, *B*167, *B*205–*B*209, *B*235–*B*237) which cluster around the end of the β-barrel domain that is distal to the di-copper ion centre (Fig. 6). The segment Pro*B*26–Asp*B*30 resides at the very N-terminus of helix I of the membrane anchor and presumably already contacts the polar region of the lipid bilayer. Gly*B*167 and Ser*B*205–Glu*B*209 are parts of complex loops which link β-strands 4 with 5 and 8 with 9. Finally, the epitope segment Ser*B*235–Glu*B*237 is the N-terminal part of helix HC, whose C-terminal location places this secondary-structure element most distal to the membrane surface. With the exception of CDR-H2, all CDR loops of the Fv fragment are involved in antigen recognition.

Despite the number of discontinuous segments contributing to the formation of the 7E2–COX complex, the epitope and antigen-binding surfaces are surprisingly small: only 352 Å^2 of the surface of the 7E2 Fv fragment is occluded from solvent access when complexed with the COX antigen (V_L, 201 Å^2; V_H, 147 Å^2). The recognized epitope on SU II is similarly small, with an occluded surface area of 392 Å^2. In contrast, other structurally characterized complexes between soluble protein antigens and antibodies show that 600–900 Å^2 of the antigen-binding site or epitope are occluded upon complexation (Davies & Cohen, 1996). The relatively small antigen-binding site and epitope of the 7E2 antibody might be a consequence of steric hindrance exerted on antibody binding by the membrane context of COX. A model of the 7E2–COX complex in a lipid bilayer (Fig. 6) shows that the epitope emerges from the membrane surface almost perpendicularly. Owing to 'steric crowding' between the membrane surface and epitope, several regions of the 7E2 V_L domain, namely the framework residues AspL1–GluL3 and SerL65–GlnL70 and parts of CDR-L1 (SerL26–AsnL28), come into close contact with the polar surface of the

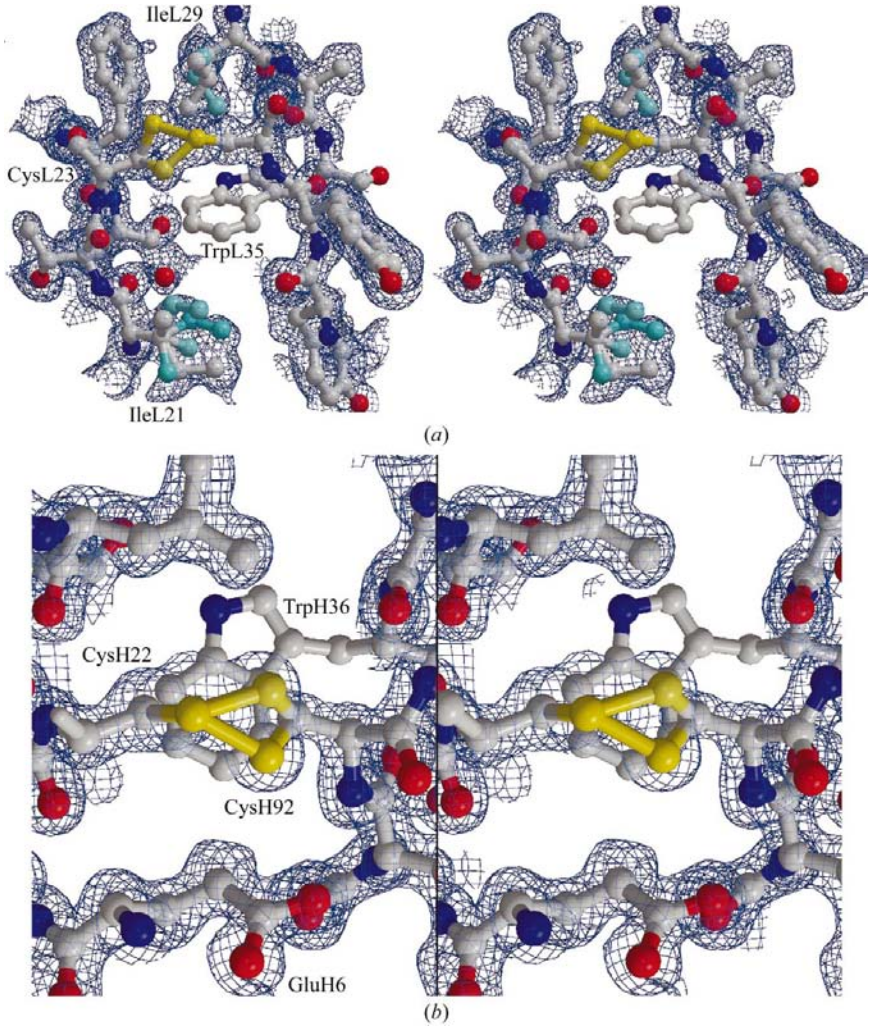

Figure 5
Stereoviews showing the structural flexibility of the core regions in the 7E2 Fv fragment. (*a*) The intrachain disulfide bridge of the V_H domain. The $3|F_o| - 2|F_c|$ electron density is contoured at 0.50 e$^-$Å^{-3}. (*b*) The hydrophobic core region of the V_L domain. The $3|F_o| - 2|F_c|$ electron density is contoured at 0.25 e$^-$ Å^{-3}. For clarity, electron density was omitted for TrpL35.

lipid bilayer or detergent micelle. One of these regions, SerL65–GlyL66, dislocates its backbone by 1.2 Å towards the hypothetical membrane centre in the 7E2–COX complex when compared with the uncomplexed 7E2 Fv fragment. Whether this structural change originates from interactions between the antibody fragment and the detergent micelle around COX or just from packing differences in the two crystal forms is unclear.

The 7E2 Fv fragment exhibits a high degree of pre-existing surface complementarity towards its cognate epitope: the C^{α} traces of both the uncomplexed Fv fragment and its complex with the two-subunit COX (PDB code 1ar1) superimpose with an r.m.s. deviation of 0.68 Å for 225 equivalent C^{α} positions. This deviation mainly arises from a rotation of the V_H domain by 1.1° along the V_H/V_L interface which is not accompanied by significant conformational changes of residues at the interface region. An eminent feature of the antigen-binding site is the protruding tyrosine cluster TyrL32, TyrL92 and TyrH98. The hydroxyl groups of TyrL32 and TyrH98 are oriented in parallel and intimately involved in hydrogen bonds to His*B*29 ND2 (TyrL32, 3.5 Å), Asp*B*207 OD1 (TyrL32, 3.5 Å), Asp*B*207 OD2 (TyrH98, 2.9 Å), Ser*B*205 OG (TyrH98, 3.1 Å) and Ser*B*205 O (Tyr H98, 2.9 Å); TyrL92 only makes some minor van der Waals interactions with the pyrrolidine group of Pro*B*26 (occluded area 10 $Å^2$) and presumably stabilizes the orientation of the aromatic groups of TyrL32 and TyrH98. The remainder of CDR-L3 is not involved in any further interactions with the antigen; its unique conformation (see above) is probably only required for pre-stabilizing the 3:3 loop conformation of CDR-H3. Consequently, only minor side-chain readjustments of 0.7 and 1.4 Å are observed for TyrL32 and TyrH98, respectively. With an occluded area of 132 $Å^2$ or 37.5% of the antigen-binding site surface, CDR-H3 plays a central role in the binding of the COX antigen. The carboxyl group of GluH96 is within hydrogen-bonding distance of Ser*B*235 OG (3.2 Å) and Glu*B*237 OE2 (3.2 Å); hydrophobic packing interactions are observed between the side chains of TyrH97/Val*B*166/Ser*B*235 and TyrH98/Gly*B*167. Likewise, CDR-L2 (occluded area 93 $Å^2$, 26.4%) makes hydrogen bonds to Glu*B*209 OE1 (TyrL49 OH, 3.6 Å), Glu*B*209 N (TyrL49 OH, 3.6 Å), Asp*B*207 OD1 (AsnL50 ND2, 3.4 Å) and Gln*B*208 NE2 (LysL52 NZ, 2.9 Å; ThrL53 OG1, 2.7 Å); other hydrogen bonds are found for TyrL30 OH–Asp*B*30 OD1 (2.7 Å), SerL31 OG–His*B*29 NE2 (2.7 Å), TyrH32 OH–Glu*B*237 OE2 (3.3 Å) and TyrH32 OH–Glu*B*237 N (3.0 Å). All of these interactions occur without significant large conformational changes of the 7E2 antibody.

Unlike the surface areas of the antigen-binding site and its epitope, the contribution of hydrophilic atoms to the surfaces of the antigen-binding site (47%) and the epitope (33%) as well as the number of hydrogen bonds (16) between the 7E2 Fv fragment and COX are similar to other known complexes between antibodies and soluble protein antigens (Davies & Cohen, 1996). The small size of the antigen-binding site and the absence of strong interactions such as salt bridges which are occluded from solvent access makes it rather difficult to rationalize the high stability of this antigen–antibody complex. Certainly, the hydrogen-bonding network between 7E2 and the COX antigen might be augmented by bridging water molecules which are not resolved in the current structures of the 7E2–COX complex, but whose presence is clearly shown in high-resolution structures of other antigen–antibody complexes (Fields *et al.*, 1996; Mylvanagam *et al.*, 1998).

4. Conclusion

The high-resolution structure of the Fv fragment of the 7E2 antibody showed considerable conformational flexibility in the hydrophobic core regions of its variable domains. Whether this conformational freedom is of functional relevance is still a matter of speculation: it might allow the structurally variable CDR loops to find conformational substates which are optimal for antigen recognition or it might merely be a packing deficiency that is a relic of the tolerance towards sequence variation in the CDR loops. The small sizes of the antigen-binding site and its associated epitope can be interpreted in terms of the steric restriction imposed by the membrane context of the membrane-embedded antigen. The 7E2 anti-

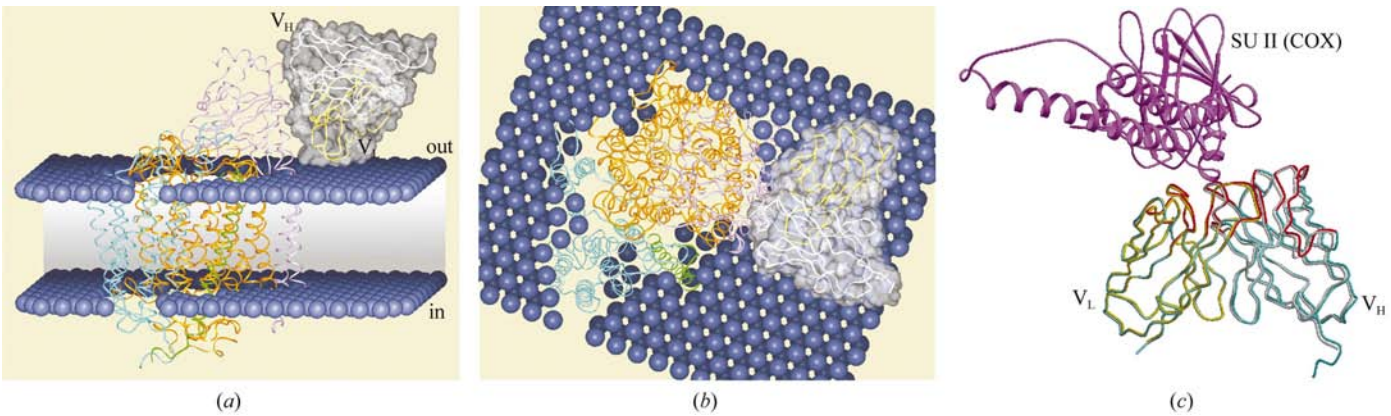

Figure 6
Structural model of the entire four-subunit cytochrome *c* oxidase–7E2 complex embedded in a hypothetical lipid bilayer. The COX subunits I–IV are shown in orange, purple, green and cyan. Each sphere represents the headgroup of an average phospholipid molecule covering 0.7 nm^2 of the membrane surface. (*a*) View from the side. (*b*) View from the extracellular side. (*c*) Structural comparison between the antigen-free and antigen-bound 7E2 Fv fragment.

body counterbalances this restriction by the use of a long CDR-L3 loop and a unique variation of the V_H/V_L packing.

The crystal packing of the unliganded 7E2 Fv fragment differs from the 7E2–COX complexes by the rather large surface areas which are involved in crystal contacts: 810 Å^2 of a total protein surface of 9406 Å^2. In the 7E2–COX complexes the interactions with the Fv fragment are dominated by the interaction with the epitope; only 268 Å^2 (tetragonal crystal form) and 136 Å^2 (orthorhombic crystal form) are derived from other Fv-mediated crystal contacts. The absence of common Fv–Fv interactions between the complexed and uncomplexed crystal forms implies that the Fv-fragment-induced crystallization is independent of unique contact areas provided by the 7E2 Fv fragment. However, it appears likely that the mostly polar surface characteristics of the framework regions are compatible with a huge variety of different crystal packing arrangements. Such a lack of predefined arrangements is not necessarily a disadvantage for cocrystallization with other detergent-solubilized membrane proteins, because the protein/detergent aggregates might select suitable crystal packings according to their steric demands. The conserved water networks which were found on the surfaces of the antibody framework regions might be generally beneficial by increasing the hydrophilicity of the exposed protein surfaces of antibody–membrane protein complexes.

The authors thank U. Ermler for discussion, V. Lamzin for helpful advice and H. Bartunik for support at synchrotron beamline BW6, HASYLAB, Hamburg. This work was supported by grants from the Fonds der Chemischen Industrie (LOE, HM).

References

Al-Lazikani, B., Lesk, A. M. & Chothia, C. (1997). *J. Mol. Biol.* **273**, 927–948.

Brünger, A. T. (1990). *Acta Cryst.* A**46**, 46–57.

Brünger, A. T. (1993). *X-PLOR Manual Version* 3.1. New Haven, CT, USA: Yale University Press.

Brünger, A. T., Leahy, D. J., Hynes, T. R. & Fox, R. O. (1991). *J. Mol. Biol.* **221**, 239–256.

Chothia, C., Lesk, A. M., Gherardi, E., Tomlinson, I. M., Walter, G., Marks, J. D., Llewelyn, M. B. & Winter, G. (1992). *J. Mol. Biol.* **227**, 799–817.

Chothia, C., Lesk, A. M., Levitt, M., Amit, A. G., Mariuzza, R. A., Phillips, S. E. & Poljak, R. J. (1986). *Science*, **233**, 755–758.

Chothia, C., Lesk, A. M., Tramontano, A., Levitt, M., Smith-Gill, S. J., Air, G., Sheriff, S. Padlan, E. A., Davies, D., Tulip, W. R., Colman, P. M., Spinelli, S., Alzari, P. M. & Poljak, R. J. (1989). *Nature (London)*, **342**, 877–883.

Collaborative Computational Project, Number 4 (1994). *Acta Cryst.* D**50**, 760–763.

Constantine, K. L., Friedrichs, M. S., Goldfarb, V., Jeffrey, P. D., Sheriff, S. & Mueller, L. (1993). *Proteins*, **15**, 290–311.

Constantine, K. L., Friedrichs, M. S., Metzler, W. J., Wittekind, M., Hensley, P. & Mueller, L. (1994). *J. Mol. Biol.* **236**, 310–327.

Dauter, Z., Lamzin, V. S. & Wilson, K. S. (1997). *Curr. Opin. Struct. Biol.* **7**, 681–688.

Davies, D. R. & Cohen, G. H. (1996). *Proc. Natl Acad. Sci. USA*, **93**, 7–12.

Eigenbrot, C., Randal, M., Presta, L., Carter, P. & Kossiakoff, A. A. (1993). *J. Mol. Biol.* **229**, 969–995.

Engh, R. A. & Huber, R. (1991). *Acta Cryst.* A**47**, 392–400.

Epp, O., Colman, P., Fehlhammer, H., Bode, W., Schiffer, M. & Huber, R. (1974). *Eur. J. Biochem.* **45**, 513–524.

Essen, L.-O., Siegert, R., Lehmann, W. D. & Oesterhelt, D. (1998). *Proc. Natl Acad. Sci. USA*, **95**, 11673–11678.

Fields, B. A., Goldbaum, F. A., Dall'Acqua, W., Malchiodi, E. L., Cauerhoff, A., Schwarz, F. P., Ysern, X., Poljak, R. J. & Mariuzza, R. A. (1996). *Biochemistry*, **35**, 15494–15503.

Frisch, C., Kolmar, H., Schmidt, A., Kleemann, G., Reinhardt, A., Pohl, E., Usón, I., Schneider, T. R. & Fritz, H.-J. (1996). *Fold. Des.* **1**, 431–440.

Harrenga, A. & Michel, H. (1999). *J. Biol. Chem.* **274**, 33296–33299.

Hunte, C. & Michel, M. (2002). *Curr. Opin. Struct. Biol.* **12**, 503–508.

Iwata, S., Ostermeier, C., Ludwig, B. & Michel, H. (1995). *Nature (London)*, **376**, 660–669.

Jones, T. A., Zou, J.-Y. & Cowan, S. W. (1991). *Acta Cryst.* A**47**, 110–119.

Kabat, E. A., Wu, T. T., Reid-Miller, M., Perry, H. M. & Gottesmann, K. S. (1991). *Sequences of Proteins of Immunological Interest.* Bethesda, Maryland: National Institutes of Health.

Kleymann, G., Ostermeier, C., Heitmann, K., Haase, W. & Michel, H. (1995). *J. Histochem. Cytochem.* **43**, 607–614.

Kleymann, G., Ostermeier, C., Ludwig, B., Skerra, A. & Michel, H. (1995). *Biotechnology*, **13**, 155–160.

Kraulis, P. J. (1991). *J. Appl. Cryst.* **24**, 946–950.

Lamzin, V. & Wilson, K. S. (1993). *Acta Cryst.* D**49**, 129–147.

Landau, E. & Rosenbusch, J. P. (1996). *Proc. Natl Acad. Sci. USA*, **93**, 14532–14535.

Laskowski, R. A., MacArthur, M. W., Moss, D. S. & Thornton, J. M. (1993). *J. Appl. Cryst.* **26**, 283–291.

Martin, A. C. R., Cheetham, J. C. & Rees, A. R. (1989). *Proc. Natl Acad. Sci. USA*, **86**, 9268–9272.

Matthews, B. W. (1968). *J. Mol. Biol.* **244**, 491–497.

May, A. C. W. & Johnson, M. S. (1994). *Protein Eng.* **7**, 475–485.

Morea, V., Tramontano, A., Rustici, M., Chothia, C. & Lesk, A. M. (1998). *J. Mol. Biol.* **273**, 927–948.

Mylvanagam, S. E., Paterson, Y. & Getzoff, E. D. (1998). *J. Mol. Biol.* **281**, 301–322.

Ostermeier, C., Essen, L. O. & Michel, H. (1995). *Proteins*, **21**, 74–77.

Ostermeier, C., Harrenga, A., Ermler, U. & Michel, H. (1997). *Proc. Natl Acad. Sci. USA*, **94**, 10547–10553.

Ostermeier, C., Iwata, S., Ludwig, B. & Michel, H. (1995). *Nature Struct. Biol.* **2**, 842–846.

Padlan, E. A. (1994). *Mol. Immunol.* **31**, 169–217.

Proba, K., Wörn, A., Honegger, A. & Plückthun, A. (1998). *J. Mol. Biol.* **275**, 245–253.

Richardson, J. S. (1981). *Adv. Protein Chem.* **34**, 167–339.

Schertler, G. F., Bartunik, H. D., Michel, H. & Oesterhelt, D. (1993). *J. Mol. Biol.* **234**, 156–164.

Schulze-Gahmen, U., Rini, J. M. & Wilson, I. A. (1993). *J. Mol. Biol.* **234**, 1098–1118.

Shirai, H., Kidera, A. & Nakamura, H. (1996). *FEBS Lett.* **399**, 1–8.

Sibanda, B. L., Blundell, T. L. & Thornton, J. M. (1989). *J. Mol. Biol.* **206**, 759–777.

Spinelli, S., Frenken, L., Bourgeois, D., de Ron, L., Bos, W., Verrips, T., Anguille, C., Cambillau, C. & Tegoni, M. (1996). *Nature Struct. Biol.* **3**, 752–757.

Steipe, B., Plückthun, A. & Huber, R. (1992). *J. Mol. Biol.* **225**, 739–753.

Suh, S. W., Bhat, T. N., Navia, M. A., Cohen, G. H., Rao, D. N., Rudikoff, S. & Davies, D. R. (1986). *Protein Eng.* **1**, 74–80.

Tomlinson, I. M., Cox, J. P. L., Gherardi, E., Lesk, A. M. & Chothia, C. (1995). *EMBO J.* **14**, 4628–4638.